Shear velocity and intrinsic attenuation variations within the Aegean lithosphere deduced from surface waves

Kassaras I (1), Louis F (1), Makropoulos K (1), Magganas A (2)

1) National and Kapodistrian University of Athens, Faculty of Geology and Geoenvironment, Department of Geophysics-Geothermics,, Panepistimioupolis, Zografou, Athens 15784, kassaras@geol.uoa.gr
2) National and Kapodistrian University of Athens, Faculty of Geology and Geoenvironment, Department of Mineralogy & Petrology, Panepistimioupolis, Zografou, Athens 15784, amagganas@geol.uoa.gr

Keywords: Rayleigh wave, Phase velocity, Attenuation, Aegean Sea

Introduction

An overall description of the lithosphere and upper mantle in the Aegean area is given by several researchers. The majority of studies on deep lithosphere and upper mantle velocity structure are based on P wave propagation (e.g. Spakman et al., 1993; Papazachos and Nolet 1997; Tiberi et al., 2000). Seismic surface waves have been used to study the shear-wave velocity variation in the Aegean (most recently Marone et al., 2004; Bourova et al., 2005; Kassaras et al., 2005; Karagianni et al., 2005). Several Q studies have been carried out in Greece. Shear and Coda waves for high frequencies have been used to study Q_b and Q_c in Greece (e.g. Kovachev et al., 1991; Hatzidimitriou, 1993). However, evident is the lack of surface wave attenuation studies, which, in contradiction to body or coda waves can provide information on the depth dependence of Q, inferring resources to understand the material and physical conditions in the lithosphere.

This paper presents a new shear velocity and attenuation model for the lower crust and lithosphere of the Aegean region, obtained by inversion of broadband surface-wave phase velocities and attenuation coefficients. We have two main motivations for conducting this study. First, knowledge of the regional structure of the Aegean lithosphere is fundamental for understanding the tectonic framework and mantle dynamics, posing constraints on possible models of deformation and evolution. Second, the exponential dependence of Q with temperature implies that attenuation tomography could explain better hot regions (high attenuation) than elastic tomography. Furthermore, elastic velocity is highly influenced by the constitution of the medium. In case of strong lateral Q variations, elastic parameters also vary. Hence, it is important to combine results of elastic and anelastic tomography. Apparently, the high rates of deformation in the Aegean constitute this region particularly interesting in this perspective.

Materials and methods

In the present study, phase velocities and attenuation coefficients of the fundamental mode of Rayleigh wave propagated across the Aegean were used. Approximately 430 teleseismic earthquakes with M>5.0, recorded during a 6 month experiment by 12 broadband stations installed in the Aegean were considered. Data from 3 GEOFON stations in south Aegean were also used. Figure 1 presents the locations of the 15 stations used.

Out of all the recorded earthquakes of epicentral distance larger than 300, waveforms generated by 386 events showing a good-quality signal at most of the stations were analyzed. Given the different sensors and recorders, the data were first corrected for the instrument

response. Phase velocities and attenuation coefficients for Rayleigh wave were determined between selected pairs of stations located on the same great circle as the epicenter, within 2-3º.

Phase velocities of the fundamental mode Rayleigh wave have been determined for periods 10-100 sec by the two-station method along 36 interstation pathways covering the Aegean region (figure 2A). The period range our measurements is not the same for all paths. This firstly arises by the fact that the instruments used were not of the same response, hence, several paths were not sampled beyond 60 sec. The second reason was that not all paths were sampled below ~20 sec, due to multiple arrivals and multipathing effects, which could not be excluded through the multiple filtering procedure. In order to encompass homogeneous sampling of the under study area, we only consider waves with periods 20-60 sec.

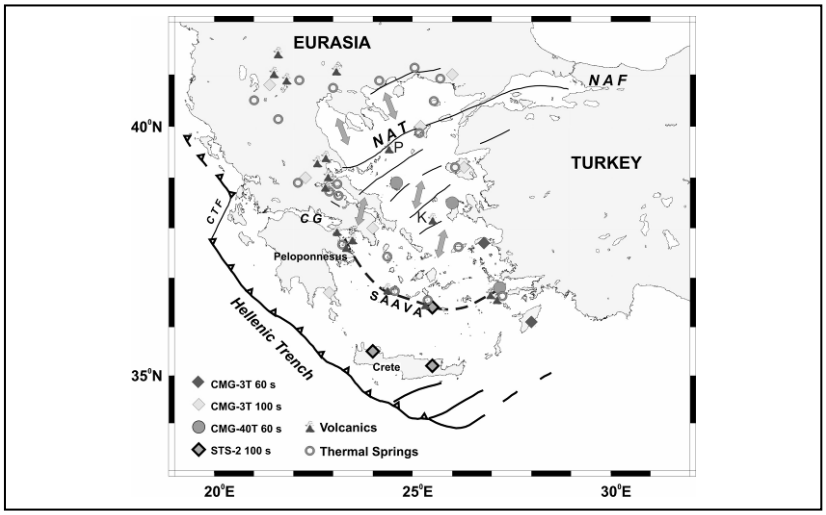

Figure 1. Map showing the location of the stations used in the present study, main active tectonic features of the Aegean, Pliocene to Recent volcanic centers and main thermal springs. Abbreviations for geographical names: CG = Corinth Gulf; NAT = North Aegean Trough; NAF = North Anatolian Fault; SAAVA = South Aegean Active Volcanic Arc; CTF = Cephalonia Transform Fault; P = Psathoura; K = Kalogeri.

For each profile the average experimental dispersion curve has been inverted to obtain 1-D horizontal average shear wave velocity models. The method of damped least-squares solution (stochastic inverse solution) was applied. To constrain our dispersion curve inversions, the depth of the Moho discontinuity was set for every path following a 2-D Moho depth model proposed by Karagianni et al., (2005). The 36 horizontal average shear velocity models determined by the inversion process were restricted between 30-120 km depth, sampling the lower crust and the upper mantle of the region.

Attenuation coefficients have been determined for periods 10-100 sec by the two-station method along 17 interstation pathways across the Aegean. The Multiple Filtering Technique (Herrmann 1973) was utilized for the identification of the fundamental Rayleigh waves and to extract group velocities and spectral amplitudes. Attenuation data were carefully verified for effects of focusing, defocusing, departures from the great-circle path and multipathing, which impact the quality of the empirical attenuation coefficient.

As expected, given the strong impact of the above effects, the largest part of the analyzed dataset exceeded the tolerance range and was consequently rejected. In conclusion, we adopted 75 interstation attenuation curves as representative of 17 paths across the Aegean (figure 2B) and calculated the average value and the corresponding standard deviation of attenuation coefficient (γ) for each period and each path. For the single period measurements, a value of 0.5×10-3 km^{-1} was chosen as a conservative error estimate.

Anelastic structures in terms of Q_b^{-1} distribution with depth were derived by stochastic inversion of attenuation coefficients (Herrmann 1994). The inversion process yielded 17 path-average Q_b^{-1} models with depth. As attenuation coefficient measurements for periods <20 and >60 sec were possible for only a few paths, we restrict those models between 30-120 km depth.

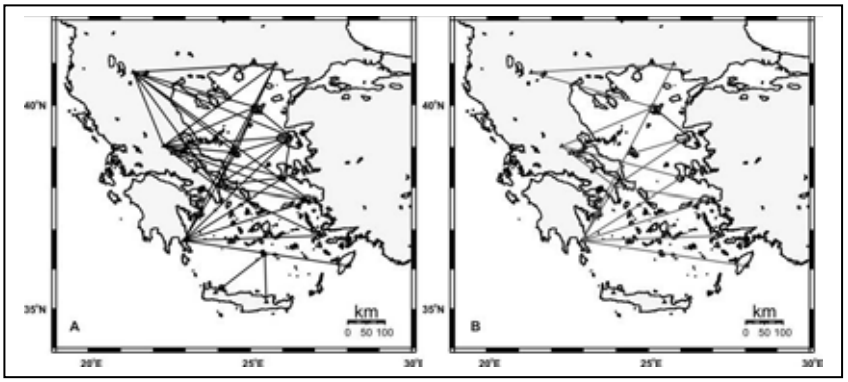

Figure 2. Paths for which phase velocities (A) and attenuation coefficient measurements (B) were obtained.

Tomography of elastic and anelastic parameters

A classical approach in surface wave tomography is to create a 3-D model in two stages. The first step is the calculation of 1-D path average models and the second step is the regionalization of these models to obtain local models. The tomographic scheme used consists of a continuous formulation of the inverse problem and the least-square criterion. The algorithm used in this study was developed by Debayle and Sambridge (2004) and it is an optimized version of the Montagner (1986) approach for continuous regionalization of surface wave path-average measurements. In the continuous regionalization algorithm, the lateral smoothness of the inverted model is obtained by assuming a priori a Gaussian correlation between neighboring points with a specified scale length L_{corr} and a scale factor σ(r). The a priori standard deviation σ(r) controls the amplitude of the perturbation allowed in the process and the horizontal correlation length is a spatial filter that constrains the lateral smoothness of the model.

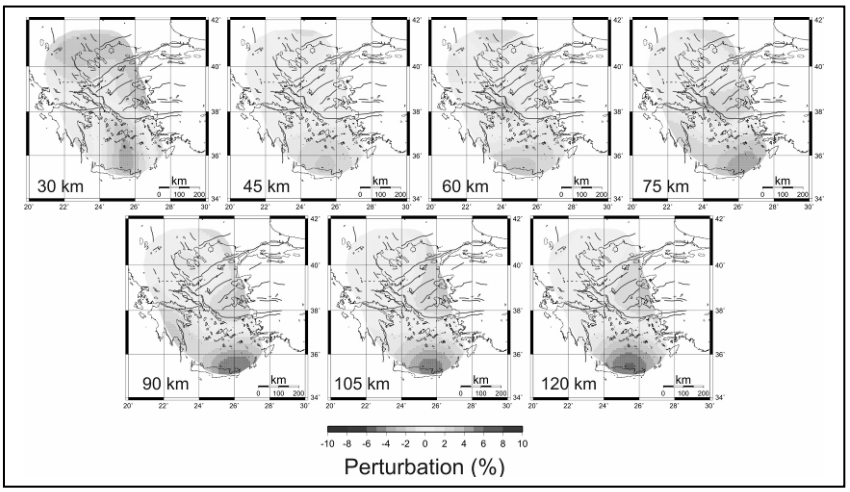

Figure 3. Tomographic slices of the shear velocity model at different depths. Tomograms start at 30 km depth. The velocity perturbations are indicated with a color scale in percent relative to a common reference model, derived from the average shear velocity at each depth.

The 36 1-D velocity models obtained were combined over a 1×1 degree grid into a single 3-D model for the lateral variations in shear velocity. The a priori standard deviation σ(r) was taken equal to 0.05 km/s, according to average phase velocity error estimate at periods 20-60 sec. The choice of an appropriate correlation length depends on the path coverage and on the period range of the inversion. After several trials L_{corr} was chosen equal to 150 km, thus favoring a smooth model considering our ray density and shortest wavelengths used (figure 3).

The 17 path-average 1-D Q_b^{-1} models with depth obtained by the inversion of attenuation coefficient curves were employed to the continuous regionalization scheme in order to obtain local Q_b^{-1}. The path-average Q_b^{-1} models with depth were combined over a 1×1 degree grid into a 3-D model for the lateral variations of Q_b^{-1}. L_{corr} was chosen equal to 150 km. Conclusions about the distribution of Q should therefore be based only on the gross features of models and fine-scale features should be ignored. σ(r) was taken equal to 5×10^{-3}. The depth range of the computed tomograms was restricted between 30 and 120 km (figure 4).

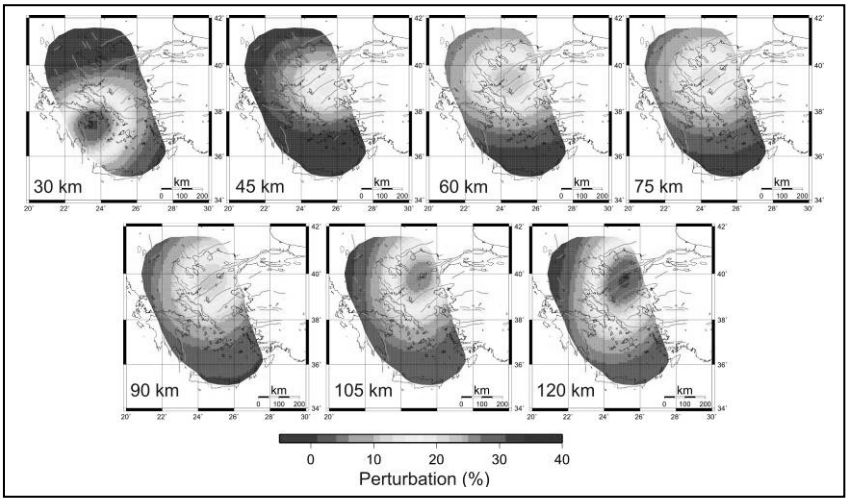

Figure 4. Tomographic slices of the Q_b^{-1} model at different depths. Tomograms start at 30 km depth. The Q_b^{-1} perturbations are indicated with a colour scale in percent relative to a common reference model, derived from the average Q_b^{-1} at each depth.

Resolution assessment of the tomographic models

The estimation of resolution is one of the main problems in seismic tomography. As the solution is not unique, the input data do not contain the information of seismic waves in every point of the medium. Although the under study area is of small dimensions, the algorithm used is inverting for local velocity over a 1×1 degree global grid and consequently the posteriori covariance matrix cannot be computed. This fact limits our ability to apply formal statistical theory to analyze the reliability and precision of the resulting tomograms. Two different approaches were applied, in order to produce a qualitative estimation of models constraint as a function of geographical position.

The Null Space Energy indicator (NSE) was used to assess the lateral resolution of the shear velocity tomograms. NSE provides an estimate of the local reliability in model space displaying areas where the data cannot reconstruct features with the desired resolution (Vesnaver 1994). This statistical tool is a function of the ray distribution and the grid size. Each component n_j of the NSE is associated with the j_{th} pixel:

$$n_j = \sum_i V_{ij}^2$$

where V_{ij} are the elements of the matrix V. The summation is performed for the indexes i of the singular values that are below the chosen threshold. We consider that two decimal points for the elements of matrix G reflect the desired actual accuracy and for this reason two orders of magnitude are the limit for the singular values that contribute positive to the solution. High values of NSE indicate solution vagueness at the corresponding pixels and vice versa. Figure 5 presents the NSE distributions along with the corresponding ray hits per cell.

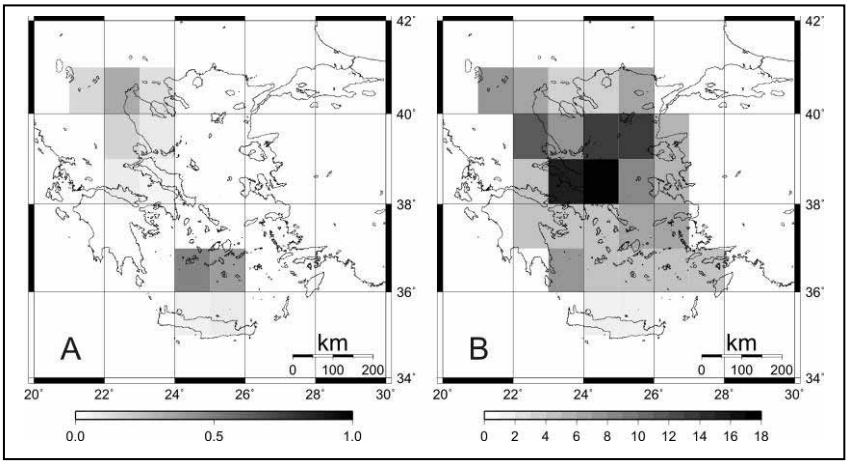

Figure 5. Null space energy (NSE) distributions (A) & the corresponding ray density map (B).

From the above figure, it is obvious that the largest uncertainties occur at the lower boundary of the model as a direct effect of limited ray coverage. In general the NSE is quite low, while in some areas it is almost zero (North East part of Figure 5A).

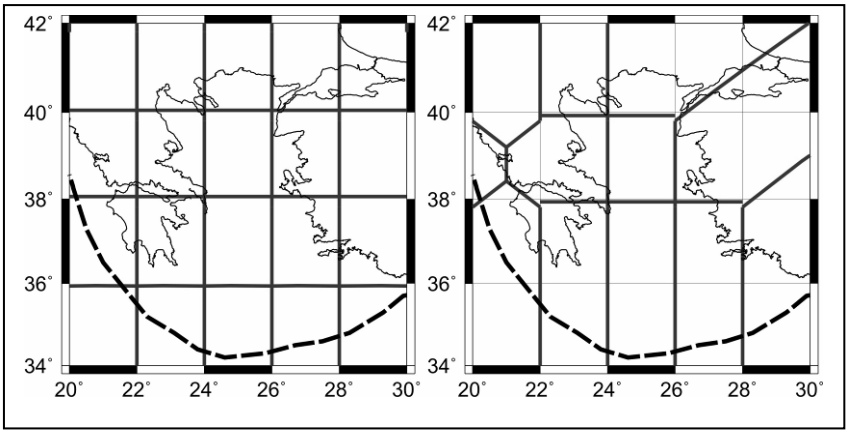

Figure 6. Voronoi diagrams to assess the anelastic model constraint as a function of geographical position. Left: Initial Voronoi diagram over a 2° × 2° grid. Right: Optimized Voronoi diagram.

In order to estimate the variation of the Q_b^{-1} model constraint provided by the ray path coverage we used Voronoi polyhedra, by applying a technique proposed by Debayle and Sambridge (2004). In two dimensions a Voronoi diagram divides the plane into a set of polygons, one about each node, such that all points in a particular cell are closer to its defining node than any other node. To produce a qualitative measure of model constraint we aim to build an optimized parameterization of the model in which each geographical point

belongs to the smallest cell for which an appropriate quality criterion is satisfied. The overall pattern of the optimized parameterization will reflect variations in model constraint.

As a starting point we built an initial Voronoi diagram falling on a 2° × 2° grid. From this starting Voronoi diagram we proceeded iteratively by building new diagrams in such a way that a particular quality criterion depending on the ray distribution is satisfied for each cell. The process of generating the new optimized Voronoi diagram is a matter of deleting nodes which do not match the criterion and then recalculating the Voronoi cells about the remaining nodes. When nodes are deleted, the neighbouring Voronoi cells inherit the area and ray paths previously contained in the deleted Voronoi cell. This makes the new cells larger on average and more likely to satisfy the quality criterion. In the final optimized diagram (figure 6) each cell denotes the size of the structures our inversion can model. As it can be seen in figure 6b, best resolution is achieved in the central region. In northern and southern region, resolution is not efficient, but it is better in the E-W direction.

Results and Discussion

The amplitude of S-wave velocity variations (approximately -3% to +8%) is compatible with phase velocity variations derived in the study of Kassaras et al., (2005). This fact implies a good compromise between experimental measurements and the inverted model. The amplitude of the velocity variations is in agreement with previous studies in the Aegean based on local and teleseismic tomography (Papazachos and Nolet, 1997; Tiberi et al., 2000) and surface wave tomography (Bourova et al., 2005).

Perhaps the most dominant feature of the model is the velocity contrast in Central and North Aegean. This tendency is evident in almost the whole depth range of the model. Papazachos and Nolet (1997), observed a low velocity zone beneath North Aegean at about 100 km depth. However, our model can not be directly compared with velocities derived from body waves tomography because of anelastic effects. Low shear velocities were observed by Bourova et al. (2005 in this area) at depths 50-120 km. The amplitude of the observed velocity contrast is between -1% and -3%. Interpretations of seismic velocity heterogeneities are generally based on thermal variations. Vs variations of 1% to 3% over distances of a few hundred kilometers, as observed in our model, can be obtained with temperature variations of 70 to 200 °C (Goes et al., 2000), which may result to melts and/or fluids circulation. Moreover, Pleistocene to Recent trachyandesitic volcanism and high heat flow, as expressed by hot springs in Central Greece (SE Thessaly and N. Evoicos Gulf), can be the result of mantle-originated magmas differentiated during their ascent through the relatively thin crust of the area (Makris et al., 2001). The southwestwards NAF propagation during the last 5 Ma, which has reached the eastern continental coast of Central Greece, may also be of significant importance to both volcanism and low velocity zone in this particular location.

High velocities are observed in continental Greece at depths 45-120 km. This is compatible with Papazachos and Nolet (1997), Marone et al., (2004), Bourova et al., (2005). The observed high velocity zone extends from north-western Greece to the Turkish coast, going through western Greece and southern Aegean and subparallel to the Hellenic trench. Marone et al., (2004) interpret this structure as the subducted lithospheric African plate, which is bounded to the east of the study area, in the region of southwestern coast of Turkey.

One of the main features of our model is a high-velocity anomaly in south Aegean, associated with the slab. However, a limited resolution and better path coverage is required to obtain constraints on the slab geometry. North of NAT, a high velocity anomaly is observed (Figure 3), possibly associated with the southern margin of the Eurasian continental lithosphere. Although null space energy is high at this part of our model (poor resolution) the pattern is compatible with a high velocity anomaly found at the same area by Papazachos and Nolet (1997).

As expected, the attenuation pattern follows that of shear velocities. Within the examined depth range (30-120 km) the amplification of perturbations in the anelastic tomograms is between 0-20 % with respect to the background model, about 2 times higher than shear

velocity perturbations, magnitude compatible with attenuation observations elsewhere (Mitchell, 1995).

Except in the case of 30 km depth, where elastic tomography is highly connected with crustal thickness, high attenuation is associated with low shear velocities, apparently in the North Aegean region. As in elastic tomography this region is about 200 km wide and extends in depth possibly deeper than our model. The resolution assessment shows that in this particular area the structures which can be retrieved are of similar dimensions, thus the possibility of an artefact intrusion is quite low.

The presence of this zone could be attributed to several reasons, including melting in the lithospheric mantle or asthenosphere and distributed deformation. Indeed, the NAF in the area and the associated intense north-south extension caused rapid tectonic instability in the area expressed in both mantle and crustal levels. NAT and Orfanos Gulf basins are their crustal surface results. NE-SW mantle olivine anisotropy (Hatzfeld et al., 2001) and extension in about the same direction suggest upper mantle deformation or flow. Recent magmatic mantle processes are manifested in the small volcanic islets of Psathura and Kalogeri of Northern and Central Aegean, respectively (Figure 1). They consist of sodic basalts derived from oceanic island basalt (OIB) asthenospheric mantle source similar in geochemical character to Pliocene basalts of Western and Central Anatolia (Pe-Piper and Piper, 2002; Fytikas et al., 1984; Innocenti et al., 2005). High heat flow in the area of N. Aegean, signified by many hot springs in its islands, as well as the above mentioned petrogenetic and tectonic processes, indicate a relatively thin crust (<28 km) or a lithospheric delamination (Al-Lazki et al., 2004; Karagianni et al., 2005). Moreover, the high attenuation mantle zone depicted clearly in the northern part of the area presumably suggests magma either underplates the crust or most possibly remains further below at lithospheric-asthenospheric mantle levels, and the lithosphere-asthenosphere boundary is within our model depths, that is at depths less than 120 km beneath northern Aegean.

At about 30 km depth, the high attenuation anomaly observed in the southern part of the study area could be associated with thermal activity from hot fluids and/or magma residing in deep crustal to lithospheric mantle levels below the South Aegean active volcanic centers, and originated in the asthenospheric mantle wedge above the dehydrating African subducted slab. Reactions of the released fluids with peridotitic lithospheric mantle can also cause serpentinization, which further may decrease the seismic velocity and increase attenuation. Low attenuation is now observed throughout the Hellenic mainland likely attributed to subducted features.

Conclusions

From the study of tomographic schemes of path-average phase velocities and attenuation coefficients of fundamental Rayleigh wave crossing the Aegean a 3-D model of shear velocity variation and a 3-D model of Q_b^{-1} variation down to 120 km were obtained.

The most prominent features in the tomograms are:

1) A low shear velocity zone in central and north Aegean, which correlates well with the derived anelastic tomograms which present high attenuation in this area. This low velocities/high attenuation zone, which indicates the lithosphere-asthenosphere boundary occurs at depths less than 120 km beneath the area, could be attributed to:
   i) High extensional strain rates related with the NAF system within the Aegean, slab roll back and distributed deformation of the upper mantle, and/or
   ii) A hot or most probably partially molten lithosheric and uppermost asthenospheric mantle, which generates subordinate Pleistocene to Recent volcanism and high heat flow in the area.
2) A high velocity/low attenuation zone in the southern part of the study area and deeper than 30 km indicating the cool subducted African lithosphere beneath the South Aegean.
3) A high attenuation zone observed in the South Aegean at about 30 km depth that probably corresponds to serpentinization, hot fluids and/or magma batches residing in deep crustal to lithospheric mantle wedge levels.

4) A low attenuation region throughout the Hellenic mainland at crustal depths, which is likely ascribed to the subducted slab.

References

Al-Lazki A.I., Sandvol E., Seber D., Barazangi M., Turkelli N. and Mohamad. R. (2004). Pn tomographic imaging of mantle lid velocity and anisotropy at the junction of the Arabian, Eurasian and African plates, *Geophys. J. Int. 158, 1024–1040.*

Bourova E., Kassaras I., Pedersen H.A. Yanovskaya T., Hatzfeld D. & Kiratzi A. (2005). Constraints on absolute S velocities beneath the Aegean Sea from surface wave analysis, *Geophys. J. Int, 160, 1006-1019*.

Debayle E. & Sambridge M. (2004). Inversion of massive surface wave data sets: model construction and resolution assessments, *J. Geophys. Res., 109, B02316, doi:10.1029/2003JB002652.*

Fytikas M., Innocenti F., Manetti P., Mazzuoli P., Reccerillo A. & Villari, L. (1984). Tertiary to Quaternary evolution of volcanism in the Aegean region, In: Dixon, J.E. & Robertson A.H.F. (eds): *The geological evolution of the eastern Mediterranean., Geol. Soc., London, Spec. Publ., 17, 687-699.*

Goes S., R. Gover & P. Vacher (2000). Shallow mantle temperatures under Europe from P and S wave tomography, *J. Geophys. Res., 105, 11,153– 11,169.*

Hatzfeld D., Karagianni E., Kassaras I., Kiratzi A., Louvari E., Lyon-Caen H., Makropoulos K., Papadimitriou P., Bock G. & Priestley, K. (2001). Shear wave anisotropy in the upper mantle beneath the Aegean related to internal deformation, *J. Geophys. Res., 106, No. 12, 30737-30753.*

Hatzidimitriou P. (1993). Attenuation of coda waves in Northern Greece, *Pure Appl. Geophys., 140, 63–78.*

Herrmann R.B. (1973). Some aspects of band-pass filtering of surface waves, *Bull. Seism. Soc. Am., 62, 129-139.*

Herrmann R.B. (1994). Computer programs in Seismology, User's manual, *St. Louis University, Missouri.*

Innocenti F., Agostini S., Di Vincenzo G., Doglioni C., Manetti P., Savascin M.Y. & Tonarini S. (2005). Neogene and Quaternary volcanism in Western Anatolia: Magma sources and geodynamic evolution, *Marine Geology, 221, 397– 421.*

Karagianni E.E., Papazachos C.B, Panagiotopoulos D.G., Suhadolc P., Vuan A. & Panza, G.F. (2005). Shear velocity structure in the Aegean area obtained by inversion of Rayleigh waves, *Geophys. J. Int., 160, 127-143.*

Kassaras I., Makropoulos K., Bourova E., Pedersen H. & Hatzfeld, D. (2005). Upper mantle structure of the Aegean derived from two-station phase velocities of fundamental mode Rayleigh waves, *The South Aegean Active Volcanic Arc, Developments in Volcanology, Volume 7, Hardbound, ISBN 0-444-52046-5, Imprint ELSEVIER: 19-45.*

Kovachev S.A., Kuzin I.P., Shoda O.Yu. (1991). Attenuation of S waves in the lithosphere of the Sea of Crete according to OBS observation, *Phys. Earth Planet. Inter., 69, 101– 111.*

Makris J., Papoulia J., Papanikolaou D. & Stavrakakis G. (2001). Thinned continental crust below northern Evoikos Gulf, central Greece, detected from deep seismic soundings, *Tectonophysics, 341, 225–236.*

Marone F., van der Lee S. & Giardini D. (2004). Three-dimensional upper mantle S-velocity model for the Eurasia–Africa plate boundary region, *Geophys. J. Int., 158, 109–130.*

Mitchell B.J. (1995). Anelastic Structure and Evolution of the Continental Crust and Upper Mantle From Seismic Surface Wave Attenuation, *Rev. Geoph., vol. 33, no. 4, 441–462.*

Montagner J. (1986). Regional three-dimensional structures using long period surface waves, *Ann. Geophys., B, 4, 283-294.*

Papazachos C. &Nolet, G. (1997). P and S-wave velocity structure of the Hellenic area obtained by robust nonlinear inversion of travel times, *J. Geoph. Res., 102, B4, 8349-8367.*

Pe-Piper G. & Piper D.J.W. (2002). The igneous rocks of Greece, *Gebruder Borntraegen, Berlin-Stuttgard, 573p.*

Spakman W., Van der Lee S. & Van der Hilst R.D. (1993). Travel-time tomography of the European-Mediterranean mantle down to 1400 Km, *Phys. Earth Planet. Inter., 79, 3-74.*

Tiberi C., Lyon-Caen H., Hatzfeld D., Achaeur U., Karagianni E., Kiratzi A., Louvari E., Panagiotopoulos D., Kassaras I., Kaviris G., Makropoulos K. & Papadimitriou P. (2000). Crustal and upper mantle structure beneath the Corinth rift from a teleseismic tomography study, *J. Geophys. Res., 105, 28159-28171.*

Vesnaver A. (1994). Towards the uniqueness of tomographic inversion solutions, *J. of Seismic Explor., 3, 323-334.*